Modeling the Solvation Sites in Rare-Gas Matrices with the Simulated Annealing Monte Carlo Technique

Alexander Moskovsky and Alexander Nemukhin*

Chemistry Department, Moscow State University, Moscow 119899, Russian Federation

Received August 23, 1998

The formation of solvation sites of rare-gas atoms (Rg = Ar, Kr) that trap the guest molecular systems is modeled using the simulated annealing Monte Carlo technique. As the guests, two molecular species are considered namely, the simplest hydrogen-bonded intermolecular complex $(HF)_2$, and the radical SH in the excited electronic state. Both are important for investigations in the low-temperature matrices. The realistic potential energy surfaces for the simulations are constructed on the basis of spectroscopically parametrized functions for the constituting fragments and empirical solvent−solvent interaction potentials. It is shown that both examples give distinctively different pictures of the solvation sites. For the $(HF)_2@Ar_n$ clusters three types of solvation shells can be distinguished which correlate with the structures of pure argon clusters as well as with the structure in the bulk. For the $SH@Rg_n$ clusters no clear regularities are seen, and larger amounts of solvent atoms are needed to form the trapping cage.

INTRODUCTION

The microsolvation theory which considers the properties of both solvent and solute species at the discrete molecular level requires at the initial stages of the modeling the detailed knowledge of the picture of solvation shells. The arrangements of the environmental atoms of the solvent around the trapped molecule of the solute, i.e., the solvation sites, may have peculiar shapes which primarily depend on the intermolecular interaction potentials as well as on the external parameters such as temperature and pressure.

Modeling the solvation sites at the supramolecular level may be approached from two different starting points. With the known interaction potentials one can design solvation shells by adding the atoms (or molecules) of the solvent one by one to the solute moiety and searching each composition for the arrangements corresponding to the minima on the multidimensional potential energy surfaces. The formation of a solvation shell accompanying the growth of the cluster is controlled by either geometry criteria or by the observation of sharp changes in other parameters beyond interparticle distances, e.g., energy per particle. In this development the microsolvation theory meets the cluster science with relevance to experimental studies of the van der Waals clusters in the gas phase and the corresponding modeling of cluster properties.[1−3]

Another way to construct the solvation sites is to start from the bulk, more specifically, from a large fragment of the crystal formed by the solvent particles frozen at lattice positions and the solute molecule embedded into some vacancy. By assuming the interaction potentials, one can find the relaxed geometry of the system and can distinguish by certain criteria the solvation sites for the nearest vicinity of the solute molecule. Such an approach models the matrix-isolated systems that are widely studied experimentally in cryochemistry.

The difficulties in realization of both programs are essentially the same. First, the reliable potential energy surfaces (PESs) should be constructed for the systems under study, and second, an efficient search of the stationary points on the multidimensional flat PES should be organized. In this article we illustrate the computational aspects of the second issue, namely, the search for the global and local minima describing solvation sites; specific systems are used as examples. We do not concentrate here on the PES construction, but only mention that because of weak and highly anisotropic solute−solvent and solvent−solvent interactions these surfaces are very complicated and contain an enormous number of stationary points.

From the computational point of view the problem of finding the solvation sites with the known interaction potentials presents a broad field of the molecular modeling program that addresses searches of stationary points on the flat multidimensional PES. The conformational analysis of polymeric molecules can be mentioned first of all. The common difficulty of all these applications is the treatment of multiple local minima on the PESs that possess close energies, which are separated by energy barriers. In the applications considered here, different minimum energy points on the potential surfaces refer to different trapping sites for the solute molecule inside the solvation shells.

Several algorithms to find the stationary points on multidimensional PESs are described in the literature.[4−9] In this work we rely on the simulated annealing Monte Carlo procedure[4] which is based on the random walking over the coordinate space of all particles in the system. The Metropolis algorithm is used for each temperature value and the computational scheme includes the following steps:

1. Select initial temperature T high enough that the system is allowed to migrate over energy barriers.

2. Select a trial geometry configuration of the system that will be considered at the current step as the old set of coordinates.

10.1021/ci9802169 CCC: $18.00
Published on Web 02/04/1999

3. A new trial geometry configuration is created by the random displacement of one or several atoms from the starting (old) positions. In practice these displacements are uniformly distributed within the cube centered at the old atom positions.

4. Compute the energies of the old (E_{old}) and new (E_{new}) geometry configurations.

5. If $E_{new} < E_{old}$, then the new trial configuration is accepted for the next step.

6. If $E_{new} < E_{old}$, the trial configuration is accepted with probability $p = \exp(-(E_{new} - E_{old})/kT$, where k is the Boltzmann constant. A uniform random number is generated between 0 and 1 and if this number is greater than p, the trial configuration is accepted. At the next step of the algorithm this configuration will be initial. If the trial configuration is rejected, then the old configuration is recounted as initial for the next step.

The distributed sets of atomic coordinates are generated consequently with gradually lowering temperature. At high T values the system is allowed to migrate over the energy barriers, but at low temperature the random walking occurs in the vicinity of an energy minimum.

There are no common recommendations about how to lower the temperature during the simulations. To some extent, the success of the search of the global minimum on PES depends on temperature manipulations. Often the temperature for a new cycle ($i + 1$) of the simulated annealing algorithm is linearly scaled as $T_{i+1} = \lambda T_i$, where parameter λ is chosen by the trial and error strategy. More sophisticated approaches involve lowering the temperature, for instance, on the basis of the computed heat capacity of the system.[4] We apply here the linear scaling by varying the parameter λ close to 1. Because there is no guarantee that the minimum on PES found at the end of the computational procedure is the global minimum, the procedure must be repeated with a different temperature lowering law and with the different starting geometry configuration.

We consider here two specific systems for the calculations, both are important for practical purposes. First, the formation of solvation shells of argon atoms around the hydrogen fluoride dimer is studied, namely, the $(HF)_2@Ar_n$ ($n \leq 20$) heteroclusters are considered. This system is an important example of the solvent (Ar) weakly interacting with the solute $(HF)_2$ which in turn presents the intermolecular hydrogen-bonded complex. Formation of the solvation shells of argon atoms around the hydrogen fluoride monomer HF by a stepwise addition of argon atoms was documented,[10−12] however, for the dimer only the first steps in modeling various trapping sites inside argon matrices by using the molecular dynamics simulations were considered.[13−15] The second system which models the solvation shells of the SH radical in argon and krypton environments is interesting with respect to the related simulations of the fluorescence spectroscopy of SH in the corresponding matrices.[16,17] It is important to note that in this case the search through the excited electronic state potential surface $SH(A^2\Sigma^+)@Rg_n$ is performed. In both examples, the reliable PESs are used consistent with the data of high-resolution molecular spectroscopy for the small (three−four atomic) complexes constituting the fragments of large heteroclusters.

$(HF)_2@Ar_n$ Clusters. The potential for the $(HF)_2@Ar_n$ clusters is written as the sum of contributions from the $(HF)_2$, $(HF)_\alpha$−Ar_i ($\alpha = 1,2$; $i = 1,...,n$) and Ar_i−Ar_j ($i,j = 1,...,n$) interactions:

$$V = V_{(HF)_2} + \sum_{\alpha,i} V_{HF_\alpha - Ar_i} + \sum_{i<i} V_{Ar_i - Ar_j}$$

For the solvent−solvent Ar−Ar potential we used the pairwise representation of the Aziz−Chen type[18] (see Appendix A).

The potential surface of the HF dimer $V_{(HF)_2}$ was modeled by the Quack−Suhm SQSBDE analytical function, parameters of which were adjusted following the results of high-level ab initio calculations corrected by the data on spectroscopic information available for this hydrogen-bonded complex.[19] This multiparameter potential depends explicitly on all six internal coordinates of $(HF)_2$, neither of which were fixed in our simulation. The solute−solvent Ar−HF potential (see Appendix B) was constructed on the basis of the diatomics-in-molecules scheme with a balanced treatment of neutral and ionic contributions to the intermolecular interaction.[11] Consistent with the available spectroscopic information for the Ar···HF van der Waals complex (Table 1), this potential describes the double-well relief of the surface with the lowest minimum (0.027 eV) corresponding to the linear arrangement Ar···HF, whereas another minimum (0.013 eV) refers to the other-sided linear configuration HF···Ar (Table 1). It has been shown before[14,15] that such a scheme allows one to reproduce the observed vibrational spectra of the HF dimer either inside the argon matrix or trapped on the surface of the argon nanoclusters. For each cluster $(HF)_2@Ar_n$ ($n = 1,..,20$) consequently generated by adding argon atoms to the preceding $(HF)_2@Ar_{n-1}$ system, we have applied the simulated annealing Monte Carlo algorithm described above and created the corresponding equilibrium geometry configurations. Typically about 10 calculations with different starting positions and different temperature variations for each cluster size were necessary to ensure validity of results obtained. The number of iterations for the Metropolis algorithm was varied within the range 10 000−100 000. Temperature was lowered from 60 to 100 K to 4−10 K by the linear scaling law $T_{i+1} = \lambda T_i$; where λ was about 0.90−0.98. In some cases the results of the Monte Carlo procedure were verified by the steepest descent minimization.

In total about 70 minimum energy configurations for the $(HF)_2@Ar_n$ ($n = 1,..,20$) clusters were detected among which we selected those corresponding to the lowest energies for each cluster. Presumably they refer to the global minima on the respective PES. We discuss here only some of the

Table 1. Binding Energies of the Solvent−Solvent (Ar−Ar, Kr−Kr), Solvent−Solute (Ar−HF, Ar−HS, Kr−HS) and Intrasolute ($(HF)_2$, HS) Interactions

species	binding energy, eV
Ar···Ar	0.012
Kr···Kr	0.017
Ar···HF	0.027
HF···Ar	0.013
Ar···HS	0.109
HS···Ar	0.087
Kr···HS	0.212
HS···Kr	0.174
$(HF)_2 \rightarrow HF + HF$	0.217
$SH(A^2\Sigma^+) \rightarrow S + H$	1.1

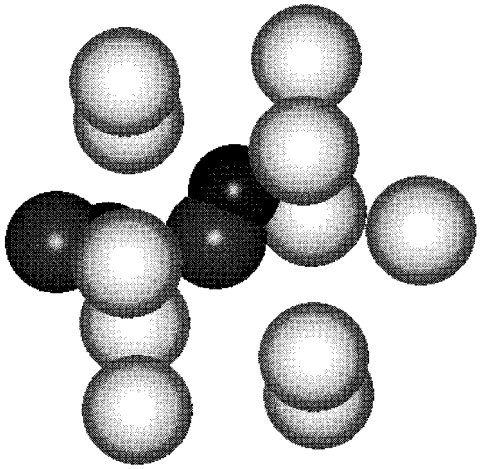

Figure 1. The structure of the $(HF)_2@Ar_{11}$ cluster.

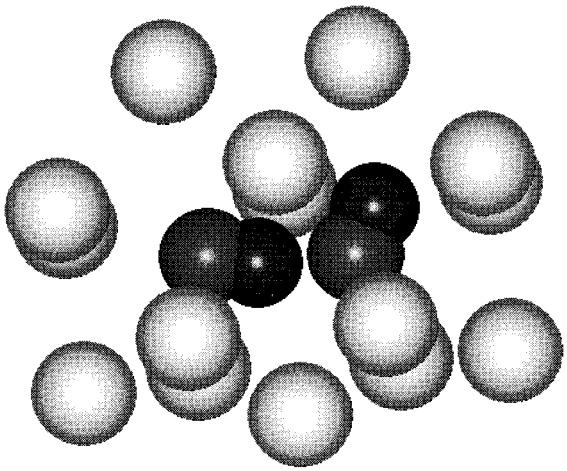

Figure 2. The structure of the $(HF)_2@Ar_{15}$ solvation site.

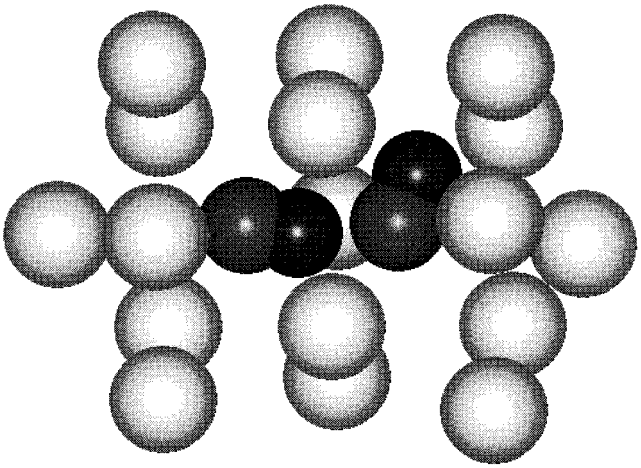

Figure 3. The structure of the $(HF)_2@Ar_{17}$ solvation site.

findings that directly refer to the solvation sites. By considering geometry configurations of the sequence of clusters, three most interesting structures can be distinguished, namely those with $n = 11$ (Figure 1), $n = 15$ (Figure 2) and $n = 17$ (Figure 3). For $n < 11$ there is no sign of proper capture of the HF dimer by the environmental atoms, and solvation shell is not completed. However for $n = 11$ (Figure 1) one can recognize a familiar motive of the Ar_{13} icosahedral cell with two argon atoms replaced by the guest complex $(HF)_2$. It is interesting that the HF dimer enters the cage from the side of the so-

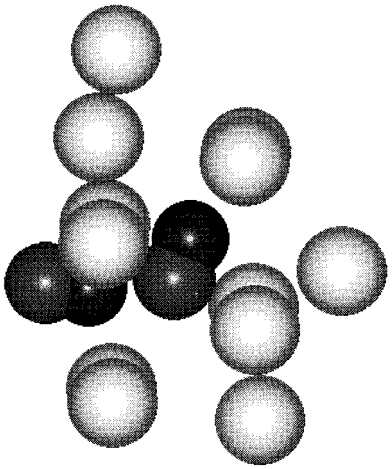

Figure 4. The structure of the $(HF)_2@Ar_{12}$ cluster. Compared to the configuration shown in Figure 1, an additional argon atom occupies a position outside the solvation site.

called "free" (not involved into the hydrogen bonding) monomer subunit HF, while another, so-called "bound" subunit HF stays mostly beyond the cage.

Addition of argon atoms to the cluster $(HF)_2@Ar_{11}$ up to $n = 15$ does not lead to noticeable changes with respect to formation of solvation sites: the most favorable arrangements of the solvent atoms correspond to their attachments to the sides of the 11-atomic icosahedron. Comparison of Figure 1 and Figure 4 showing the minimum energy structures for $n = 11$ and $n = 12$, respectively, illustrates the above statement.

Qualitatively, a new feature appears for $n = 15$ (Figure 2). In this case the dimer is completely captured by the solvent. An important observation is that practically the same configuration was distinguished as a trapping site for the HF dimer in the argon matrix when the first solvation shell was extracted from the large cluster modeling the bulk (sf. Figure 2 of ref 13). A new rearrangement of the solvation site is observed for $n = 17$ (Figure 3). In this case the intermolecular complex is also completely trapped by the solvent shell, but the shape of the shell is distinctively different from that of $n = 15$. Addition of more argon atoms to the cluster $(HF)_2@Ar_{17}$ up to $n = 20$ does not change the structure of the solvation site—the solvent atoms occupy positions around the site shown in Figure 3 without rearrangement of the closest environment. We can therefore conclude that three types of solvation shells for the hydrogen fluoride dimer inside argon are distinguished.

SH@Rg$_n$ (Rg = Ar, Kr) Clusters. The excited electronic state PES for the SH@Rg$_n$ (Rg = Ar, Kr) clusters is constructed as a sum of Rg_i—Rg_j contributions[20] and a sum over SH−Rg_i interactions:[21]

$$V = \sum_i V_{SH-Rg_i} + \sum_{i<j} V_{Rg_i-Rg_j}$$

The detailed description of these potentials is given in Appendices A and B. The empirical potential for SH···Rg suggests[21] that the S−H distance is fixed at the corresponding eqilibrium value. The three-atomic potentials have the double-well shape with the linear arrangements Rg···HS and HS···Rg corresponding to the lower and higher energy isomers, respectively. The well depths are collected in Table 1.

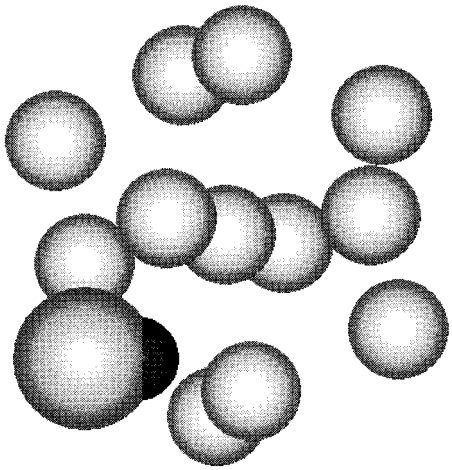

Figure 5. The structure of the SH@Kr_{12} cluster.

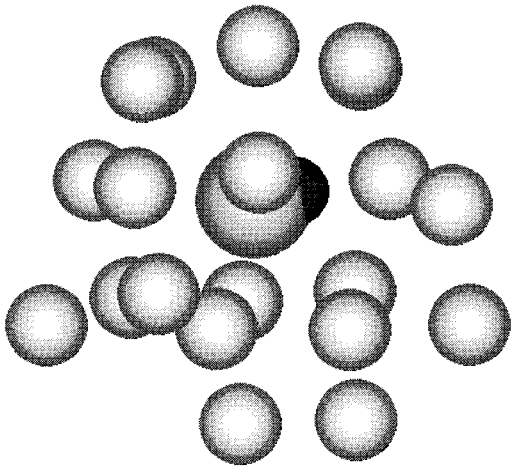

Figure 6. The structure of the SH@Kr_{22} solvation site.

The simulated annealing Monte Carlo procedure was used to search the global minimum structures for a series of clusters SH@Rg_n (n = 4, 10, 11, 12, 13, 14, 20, 22, 34, 55). The temperature was varied from 300 to 100 to 10 K, and the number of iterations in the Metropolis algorithm was 10^5-10^6 depending on cluster size.

The attempts to apply the same strategy to form the trapping sites as in the case of $(HF)_2@Ar_n$ (or in the case of $HF@Ar_n$[11]), to build the shells around SH by adding the rare-gas atoms one by one have failed. For both solvents (Ar and Kr) the guest molecule SH prefers to escape from the cage of the host atoms if their number is not large enough. Figure 5 illustrates this observation: one can see the almost completed perfect icosahedron (without one atom) of the rare-gas cluster Rg_{12} apart from the molecule SH. Only if the number of solvent atoms is considerably increased up to 22 for Kr (Figure 6) or 34 for Ar (Figure 7) does the guest molecule reside inside the shell. Remarkably, these configurations show no evidence of regularities typical for the perfect rare-gas clusters; the shells pictured in Figures 6 and 7 may be called amorphous.

Another attempt to model the matrix was made by starting from the large block of the face-centered cubic (fcc) rare-gas lattice, placing the guest molecule inside the single, double, or triple substitutional site, and calculating the equilibrium geometry configurations with the fixed positions of the outermost solvent atoms. In these cases we obtained

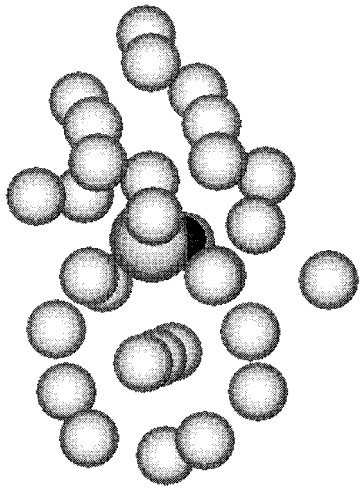

Figure 7. The structure of the SH@Ar_{34} solvation site.

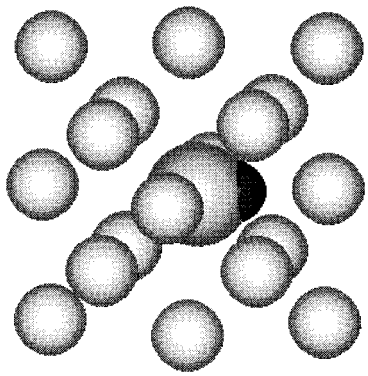

Figure 8. The structure of the solvation site SH@Rg_n obtained when starting from the fcc rare-gas lattice.

arrangements (practically common for both Ar and Kr) shown in Figure 8, but only slight distortions among the nearest environments were detected.

CONCLUSIONS

We show in this paper how the simulated annealing Monte Carlo technique can be used to search the configurations of global potential energy surface minima that describe the solvation sites for the different by their physical origin systems. Table 1 lists the binding energies of the constituting species subdivided into the solvent−solvent (Rg−Rg), solvent−solute (Rg−HF or Rg−SH), and intrasolute ($(HF)_2 \rightarrow HF + HF$ and $SH(A^2\Sigma^+) \rightarrow S + H$) classes.

For $(HF)_2@Ar_n$, $n = 1-20$, the solvation shells are formed around the hydrogen-bonded molecular complex with the binding energy only an order greater than the solvent−solute and solvent−solvent interaction energies. Nevertheless, an influence of the solvent on the structure of the guest species is almost negligible; in particular, the geometry of the complex $(HF)_2$ practically remains unaffected by the solvent. Three types of solvation sites were found for $(HF)_2@Ar_n$ with n = 11, 15, 17 (Figures 1−3). It is important to note that one of the structures (n = 15) with a completely trapped guest system practically coincides with the first solvation shell typical for the bulk (Figure 2 of ref 13). On the other hand, no configurations of the type shown in Figure 3 (n = 17) were distinguished when the matrix was modeled.[13] Another interesting finding is that the arrangements of the

solvent atoms (Ar) around the trapped species obviously show the regularities typical for pure argon clusters.

This is not the case for the SH@Rg_n particles. The final obtained configurations of the clusters which correspond to the trapping of the SH radical inside the solvation shell, first, contain larger number of solvent atoms (22 and 34), and second, show no regularities of the pure rare-gas clusters (Figures 6 and 7). The solvent−solute interaction strength is higher than in the previous case (Table 1) and that is probably the reason for a greater impact on the structure of the solvation sites. When the modeling of solvation sites is started from the large fragment of the lattice and the outermost atoms are kept fixed, we can obtain the regular structures for the heteroclusters (Figure 8), however, no similarities between the results of the "cluster" and "bulk" approaches are seen.

Our belief that the qualitative conclusions drawn in this paper with respect to the structure of the solvation sites are correct resides on the argument that the crucial factors for such modeling solvent−solute interaction potentials have been preliminarily tested by very demanding spectroscopic properties of the small van der Waals clusters (Ar···HF, Rg···SH). The potential of solvent−solvent interactions (Rg−Rg) should be considered as accurate enough for the present applications. Therefore, the realistic potential energy surfaces have been employed, and a careful application of the simulated annealing Monte Carlo technique allows us to arrive at the pictures of the solvation sites presented in this work.

ACKNOWLEDGMENT

This work was supported in part by a grant from the Russian Basis Research Foundation (project 96-03-34255).

APPENDIX A. SOLVENT−SOLVENT INTERACTION POTENTIALS

For the Rg_i—Rg_j (Rg = Ar,Kr) interaction potentials the traditional functions of Aziz−Chen[18] and Aziz−Slaman[20] type were used:

$$V_{Rg-Rg}(R) = \epsilon\cdot\left[\left(A\cdot\left(\frac{R}{R_m}\right)^n\cdot\exp(-\alpha\cdot(R/R_m) + \beta\cdot(R/R_m)^2\right) - \left(\frac{C_6}{(R/R_m)^6} + \frac{C_8}{(R/R_m)^8} + \frac{C_{10}}{(R/R_m)^{10}}\right)\right]\cdot f(R)$$

$$f(R) = \begin{cases} \exp(-(1-(D\cdot R_m)/R)^2), & \frac{R}{R_m} \le D \\ 1, & \frac{R}{R_m} > D \end{cases}$$

The parameters used for the Rg—Rg interactions are as follows:

For $(HF)_2$@Ar_n (ref 18): $R_m = 3.759$ Å, $\alpha = 16.345655$, $\beta = 0$, $n = 2$, $D = 1{,}4$, $C_6 = 1.0914254$, $C_8 = 0.6002595$, $C_{10} = 0.3700113$, $A = 9.502721\cdot10^6$, $\epsilon = 99.6$ cm^{-1}.

For SH@Ar_n (ref 20): $R_m = 3.7565$ Å, $\alpha = 10.77874743$, $\beta = -1.812004$, $n = 0$, $D = 1.36$, $C_6 = 1.10785136$, $C_8 = 0.56072459$, $C_{10} = 0.34602794$, $A = 2.26210716\cdot10^5$, $\epsilon = 99.5$ cm^{-1}.

For SH@Kr_n (ref 20): $R_m = 4.008$ Å, $\alpha = 9.39490495$, $\beta = -2.32607647$, $n = 0$, $D = 1.28$, $C_6 = 1.08822526$, $C_8 = 0.53911567$, $C_{10} = 0.42174119$, $A = 1.10146811\cdot10^5$, $\epsilon = 139.8$ cm^{-1}.

APPENDIX B. SOLVENT−SOLUTE INTERACTION POTENTIALS

Ar−HF. The Ar−HF potential surface was constructed in ref 11, following the diatomic-in-molecules theory:

$$V_{Ar-HF} = (V^{\Sigma}_{ArF}\cos^2(\psi) + V^{\Pi}_{ArF}\sin^2(\psi) + V_{ArH})\cos^2(\beta) + (V_{ArF^-} + V_{ArH^+})\sin^2(\beta)$$

This formula combines contributions from Ar−F (V^{Σ}_{ArF}, V^{Π}_{ArF}, V_{ArF^-}) and Ar−H (V_{ArH}, V_{ArH^+}) diatomic fragments and the energy depends on the corresponding internuclear distances as well as on the HF and ArF orientation (ψ). Symbols Σ and Π distinguish the components of the Ar−F potential with respect to the projections of angular momentum. The parameter β governs the balance of ionic and covalent contributions at the equilibrium point ($\beta \approx 20°$).

Rg-SH. The analytic formula which describes dependence of the potential on the distance between the SH center of mass to Rg (R_{CM}) and on the angle between R_{CM} and the SH-axis is given in ref 21:

$$V = \sum_i V_{SH-Rg_i} + \sum_{i<j} V_{Rg_i-Rg_j}$$

$$V_{SH-Rg}(R_{CM}, \theta) = V_0(R_{CM})[1 - f(\theta)] + V_{sp}(R_{CM})f(\theta) \qquad 0 \le \theta \le \theta_{sp}$$

$$V_{SH-Rg}(R_{CM}, \theta) = V_{sp}(R_{CM})[1 - g(\theta)] + V_{\pi}(R_{CM})g(\theta) \qquad \theta_{sp} \le \theta \le \pi$$

The V_0, V_π, and V_{sp} are radial cuts of the potential for $\theta = 0$, $\theta = \pi$, and the θ corresponding to saddle point angle (θ_{sp}).

For each cut

$$V(R_{CM}) = D[\exp(-\alpha_2(R_{CM} - R'_e)) - 2\exp(-\alpha_1(R_{CM} - R_e))]$$

where

$$R'_e = R_e + \frac{1}{\alpha_2}\ln\left(\frac{2\alpha_1}{\alpha_2}\right)$$

and

$$D = \frac{D_e}{2(1 - \alpha_1/\alpha_2)}$$

Functions $f(\theta)$ and $g(\theta)$ are switching functions for the ranges $0 \le \theta \le \theta_{sp}$ and $\theta_{sp} \le \theta \le \pi$, respectively. If the variable x is introduced

$$x = \frac{\exp(\lambda_1\theta) - 1}{\exp(\lambda_1\theta_{sp}) - 1}$$

for $0 \le \theta \le \theta_{sp}$,

$$x = \frac{\exp(\lambda_2(\theta - \theta_{sp})) - 1}{\exp(\lambda_2(\pi - \theta_{sp})) - 1}$$

Table B1. Parameters Used for the SH−Ar Potential Function[21]

parameter	$\theta = 0$	$\theta = \theta_{sp}$	$\theta = \pi$
R_e (au)	6.4575	8.0911	4.18
α_1	0.7117	0.2730	1.5
α_2	2.4947	1.2724	0.762
D_e (cm^{-1})	877.2	202.9	700
f_{xx}	7.254	−1.0	
g_{xx}		6.75	−7.11
λ_1	−0.6440		
λ_2	1.000		
θ_{sp} (saddle point)	92.8°		

Table B2. Parameters Used for the SH−Kr Potential Function[21]

parameter	$\theta = 0$	$\theta = \theta_{sp}$	$\theta = \pi$
R_e (au)	6.1686	7.5892	4.14
α_1	0.9581	0.5212	1.85
α_2	2.7668	2.6900	0.8625
D_e (cm^{-1})	1706.2	158.9	1400.0
f_{xx}	7.4308	−1.0	
g_{xx}		6.75	−7.11
λ_1	0.8269		
λ_2	1.000		
θ_{sp} (saddle point)	64.0°		

for $\theta_{sp} \le \theta \le \pi$, the functions $f(x)$ and $g(x)$ have the same expression, i.e.,

$$f(x) = \frac{a}{2}x^2 + \left(10 + \frac{b}{2} - \frac{3a}{2}\right)x^2 + \left(\frac{3a}{2} - b - 15\right)x^4 + \left(6 + \frac{b}{2} - \frac{a}{2}\right)x^5, \quad 0 \le x \le 1$$

with parameters $a = f_{xx}(0)$ and $b = f_{xx}(1)$.

The complete list of parameters for the SH−Ar and SH−Kr interactions is presented in Tables B1 and B2.[21] These coefficients have been adjusted in order to reproduce the observed high-resolution spectra of the three-atomic van der Waals complexes.[21]

REFERENCES AND NOTES

(1) Hoare, M. R. Structure and dynamics of simple microclusters. *Adv. Chem. Phys.* **1979**, *40*, 49−135.

(2) Berry, R. S.; Beck, T. L.; Davis, H. L.; Jellinek, J. Solid−liquid behavior in microclusters. *Adv. Chem. Phys.* **1988**, *70*(2), 75−138.

(3) Doye, J. P. K.; Wales, D. J.; Berry, R. S. The effect of the range of the potential on the structure of clusters. *J. Chem. Phys.* **1995**, *103*, 4234−4249.

(4) Kirkpatrick, K. S.; Gelatt, C. D.; Vecchi, M. P. Optimization by simulated annealing. *Science* **1983**, *220*, 671.

(5) Ma, J.; Straub, J. E. Simulated annealing using the classical density distribution. *J. Chem. Phys.* **1994**, *101*, 533−541.

(6) Oresic, M.; Shalloway, D. Hierarchical characterization of energy landscapes using Gaussian packet states. *J. Chem. Phys.* **1994**, *101*, 9844−9857.

(7) Schelstraete, S.; Verschelde, H. Finding minimum-energy configurations of Lennard-Jones clusters using an effective potential. *J. Phys. Chem. A* **1997**, *101*, 310−315.

(8) Wales, D. J.; Doye, J. P. K. Global optimization by basin-hopping and the lowest energy structures of Lennard-Jones clusters containing up to 110 atoms. *J. Phys. Chem. A* **1997**, *101*, 5111−5116.

(9) Naumkin, F. Y.; Wales, D. J. Influence of the atom−atom interaction anisotropy on the structure and stability of Ar_nCl_2 clusters. *Chem. Phys. Lett.* **1998**, *290*, 164−170.

(10) Liu, S.; Bacic, Z.; Moskowitz, J. W.; Schmidt, K. E. Equilibrium structures and approximate HF vibrational red shifts for Ar_nHF (n = 1−14) van der Waals clusters. *J. Chem. Phys.* **1994**, *100*, 7166−7181.

(11) Grigorenko, B. L.; Nemukhin, A. V.; Apkarian, V. A. Many-body potentials and dynamics based on diatomics-in-molecules: Vibrational frequency shifts in Ar_nHF (n = 1−12, 62) clusters. *J. Chem. Phys.* **1996**, *104*, 5510−5516.

(12) Dykstra, C. E. Modeling weak interaction elements affecting the structures and vibrational red-shifts of Ar_nHF clusters (n = 1 to ∞). *J. Chem. Phys.* **1998**, *108*, 6619−6632.

(13) Nemukhin, A. V.; Grigorenko, B. L. Modeling properties of the HF dimer in argon clusters. *Int. J. Quantum Chem.* **1997**, *62*, 55−65.

(14) Nemukhin, A. V.; Grigorenko, B. L.; Savin, A. V. Theoretical vibrational spectrum of $(HF)_2$ in argon matrices. *Chem. Phys. Lett.* **1996**, *250*, 226−231.

(15) Grigorenko, B. L.; Nemukhin, A. V. Modeling trapping sites of $(HF)_2$ in argon clusters. *Chem. Phys. Lett.* **1997**, *270*, 103−107.

(16) Zoval, J.; Imre, D.; Apkarian, V. A. Spectroscopy of SH(A−X) transition in Ar and Kr matrices: The caging of predissociation. *J. Chem. Phys.* **1993**, *98*, 1−7.

(17) Khriachtchev, L.; Petterson, M.; Isoniemi, E.; Räsänen, M. 193 nm photolysis of H_2S in rare-gas matrices: Luminescence spectroscopy of the products. *J. Chem. Phys.* **1998**, *108*, 5747−5754.

(18) Aziz, R. A.; Chen, H. H. An accurate intermolecular potential for argon. *J. Chem. Phys.* **1977**, *67*, 5719−5726.

(19) Quack, M.; Suhm, M. Potential energy surfaces, quasiadiabatic channels, rovibrational spectra, and intermolecular dynamics of $(HF)_2$ and its isotopomers from quantum Monte Carlo calculations. *J. Chem. Phys.* **1991**, *95*, 28−59.

(20) Aziz, R. A.; Slaman, M. J. The argon and krypton interatomic potentials revisited. *Mol. Phys.* **1986**, *58*, 679−697.

(21) Korambath, P. P.; Wu, X. T.; Hayes, E. F.; Carter, C. C.; Miller, T. A. Empirical potential energy surface for Ar.SH/D and Kr.SH/D. *J. Chem. Phys.* **1998**, *107*, 3460−3470.

CI9802169